Available online at www.sciencedirect.com
SCIENCE DIRECT®
Journal of Power Sources 119–121 (2003) 528–537
JOURNAL OF POWER SOURCES
www.elsevier.com/locate/jpowsour

A study on electrolyte interactions with graphite anodes exhibiting structures with various amounts of rhombohedral phase

W. Kohs[a], H.J. Santner[a], F. Hofer[b,1], H. Schröttner[b], J. Doninger[c], I. Barsukov[c], H. Buqa[a,2], J.H. Albering[a], K.-C. Möller[a], J.O. Besenhard[a], M. Winter[a,*]

[a]*Institute for Chemical Technology of Inorganic Materials, Graz University of Technology, A-8010 Graz, Austria*
[b]*Research Institute for Electron Microscopy, Graz University of Technology, Graz, Austria*
[c]*Superior Graphite Co., Chicago, IL 60606, USA*

Abstract

The lithium-ion battery anode performance of graphites with and without high amounts of rhombohedral phase in the structure has been investigated. A main outcome was that in addition to possible graphite bulk structure effects, there are also strong influences of the graphite surface and the graphite ''sub-surface'' (part of the graphite bulk at the border of the particle near the surface) on the solid electrolyte interphase (SEI) formation process and on the tendency to solvent co-intercalation into graphite. Using transmission electron microscopy with atomic resolution, we indeed could determine unique and also different surface and ''sub-surface'' morphologies for the two graphites. In case of the graphite without rhombohedral phase, unique convoluted graphene layers could be determined at the prismatic surfaces; in case of the graphite with a high rhombohedral phase content a strongly disordered, approximately 1 nm thick ''sub-surface'' layer could be determined. The anode performance depends primarily on these surface and ''sub-surface'' graphite properties and the used electrolytes. The differences in the ''sub-surface'' layer structure have a most significant influence on the performance in an ethylene carbonate/dimethyl carbonate electrolyte. The differences in surface structure and morphology are considered to have the highest impact in a propylene carbonate/ethylene sulfite-based electrolyte. For ethylene carbonate/diethyl carbonate electrolyte, the performance differences are small so that no strong dependence on surface or ''sub-surface'' structures could be observed.

Keywords: Graphite anode; Lithium-ion battery; Solid electrolyte interphase (SEI); Electrolyte additive; Rhombohedral phase

1. Introduction

Layered graphite exists in two crystallographically different forms: the hexagonal form (α- or 2H-phase), with a AB... graphene layer stacking sequence, and the rhombohedral modification (β- or 3R-phase) with a ABCABC... stacking sequence. Their crystal structures can be distinguished by X-ray diffraction (XRD, Fig. 1).

Naturally occurring graphites usually contain both modifications. The ratio of hexagonal to rhombohedral contents can be varied by certain processing. Mechanical treatments, especially milling, shearing or ultrasonic impact, result in a larger extent of the β-phase, whereas thermal annealing procedures at elevated temperatures convert the material to the thermodynamically more stable α-form. By heat treatment, it is possible to create a graphite which contains 100% α-phase, whereas this could not be achieved by mechanical measures for the β-form. So far β-phase contents in the range of approximately 30% have been reported [1].

Since the first application of graphite as anode in lithium-ion cells, effects of the β-phase on the electrochemical behaviour have been observed [2–10]. As the investigated graphites stem from different sources, various results have been obtained. However, there is general agreement that graphites containing higher amounts of the β-phase showed higher discharge (reversible) capacities than those with a lower β-phase content. It was also observed that a higher rhombohedral content makes graphites less vulnerable to co-intercalation of solvents (Section 3.2). The reason for this behaviour was thought to be mechanical processing, which does not only create more rhombohedral phase, but, in addition also a higher number of structural defects such as grain boundaries and dislocations. These defects create hindrances inside the graphite, which allow small unsolvated

* Corresponding author. Tel.: +43-316-873-8268; fax: +43-316-873-8272.
E-mail addresses: ferdinand.hofer@felmi-zfe.at (F. Hofer), martin.winter@tugraz.at (M. Winter).
[1] Co-corresponding author. Tel.: +43-316-873-8820; fax: +43-316-811-596.
[2] Present address: Paul Scherrer Institute, CH-5232 Villigen-PSI, Switzerland.

0378-7753/03/$ – see front matter © 2003 Elsevier Science B.V. All rights reserved.
doi:10.1016/S0378-7753(03)00278-7

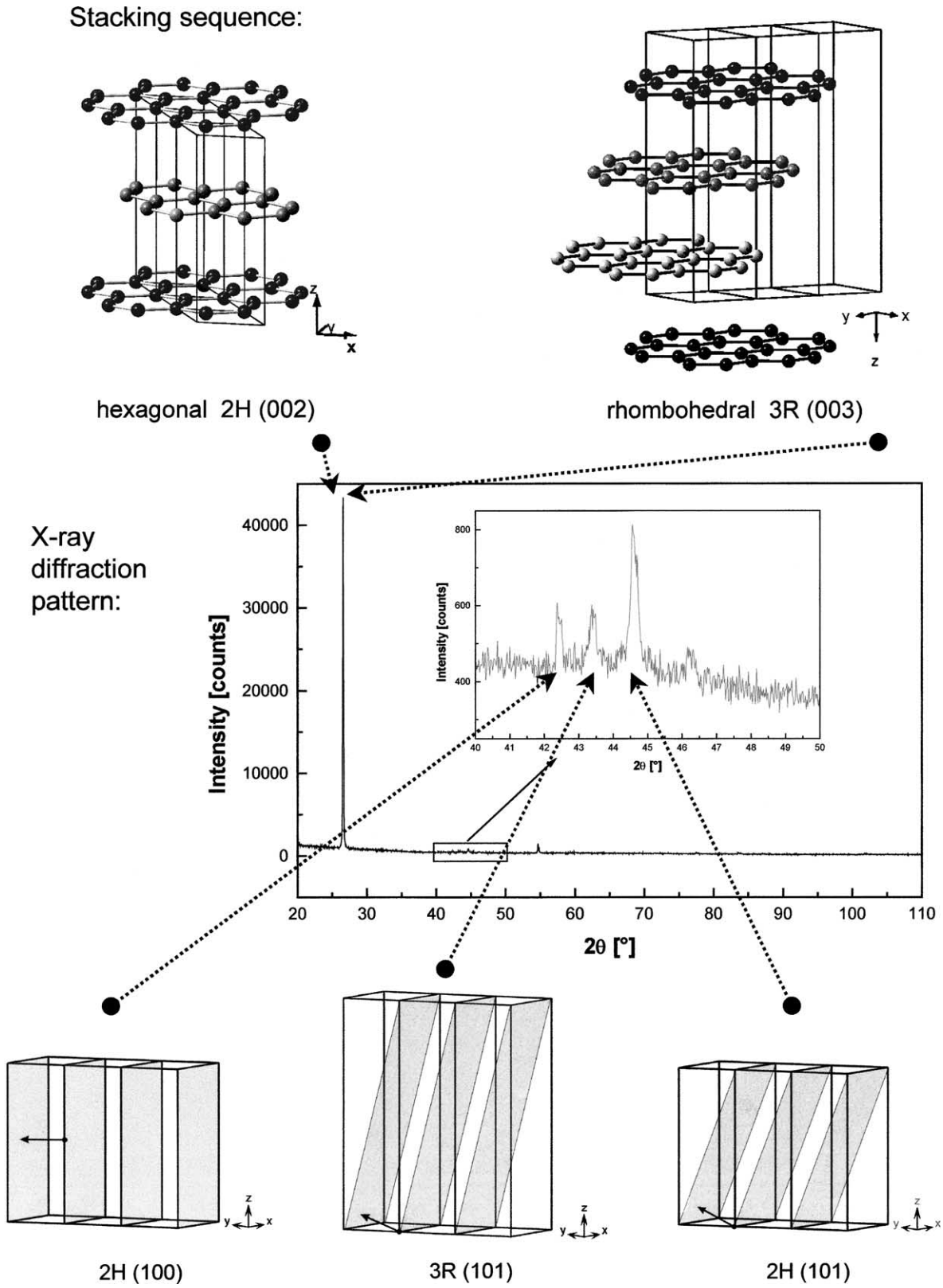

Fig. 1. (*Top*): Stacking sequence of hexagonal (2H, α-phase, sequence AB) and rhombohedral (3R, β-phase, sequence ABC) graphite. Both phases have identical interlayer distances $d_{0\,0\,\lambda}$ between the two-dimensionally infinite carbon layers and thus the 2H (0 0 2) and 3R (0 0 3) reflections coincide in the diffraction pattern. The complete XRD pattern of a typical two-phase sample is shown in the range of 20–110° (Cu Kα radiation), the inset emphasises the angular range between 40 and 50° containing the weak 2H (1 0 0), 2H (1 0 1), 3R (1 0 1) and 3R (0 1 2) reflections. (*Bottom*): Arrangement of the (1 0 0) and (1 0 1) lattice planes in the unit cells of hexagonal and rhombohedral graphite. The arrows represent the interlayer spacing vector *d*. Due to the longer *c*-axis of the rhombohedral phase (in the hexagonal setting of the rhombohedral unit cell) the 2H (1 0 1) and 3R (1 0 1) peaks can be distinguished clearly and used for an estimation of the phase content—assuming that the preferred orientation for the 2H and 3R domains is identical.

lithium cations to penetrate into the bulk graphite [3,4]. It was also proposed [2] that the higher lithium storage capacity of such graphites may be explained by lithium storage at grain boundaries in the graphite in addition to lithium intercalation between the graphene layers. On the other hand, thermal treatment can not only create hexagonal phase graphite, but also "heal" structural defects. Put in other terms: after graphite modification by thermal or mechanical means, the extent of rhombohedral or hexagonal phases in the graphite structure may be a qualitative indication for the extent of structural defects. However, it should be noted that certain graphites, for instance untreated natural graphites, may contain significant extents of rhombohedral phase by chance, but not necessarily possess a very high number of structural defects, as they have not been subjected to mechanical treatment.

We made detailed investigations of graphites with and without high amounts of rhombohedral phase. In this report, we focus on the interactions of such graphites with different electrolyte systems and discuss the formation of the solid electrolyte interphase (SEI) film in dependence on the different graphites and electrolytes used. In order to understand the electrochemical results, we made use of high resolution scanning electron microscopy (SEM) and transmission electron microscopy (TEM).

2. Experimental

Two graphite powders from Superior Graphite Co. in Chicago (USA) have been especially prepared for our investigations. One graphite has been made from natural purified flake graphite by severe mechanical processing and contains approximately 26% β-phase. Hereafter, the sample is called SO-26β. The other graphite is all-hexagonal (100% α-phase), thus called SO-100α. It has been prepared from the same starting material as the SO-26β, but by thermal treatment at temperatures >2000 °C under inert atmosphere. Currently, the detailed preparation procedures are proprietary.

The rhombohedral and hexagonal contents of the two graphites have been estimated from XRD spectra. The spectra were recorded with Cu Kα radiation, a secondary graphite monochromator and a scintillation counter on a Bruker AXS D5005 θ/θ diffractometer. A constant step width of 0.02° and a counting time of 20 s per step was applied to the samples (prepared on a rotating, low background silicon sample holder).

Anodes from the above graphites were prepared as described elsewhere [11]. The final electrodes contained 4 wt.% of poly(vinylidene)fluoride (PVDF, Mitsubishi Chemical Corp.) binder. Stainless steel grids were used as current collectors.

Ethylene carbonate (EC), propylene carbonate (PC), diethyl carbonate (DEC), dimethyl carbonate (DMC) (courtesy of Merck or Honeywell, battery grade) and $LiClO_4$ (Mitsubishi Chemical Corp., battery grade) were used as received. Ethylene sulfite (ES, Aldrich, 98%) was distilled under vacuum and dried over activated molecular sieves. Using lithium counter and reference electrodes and glass cells, cell assembly was accomplished as described elsewhere [11]. All electrolyte component handling and cell assembly was done under dry argon in a glove box.

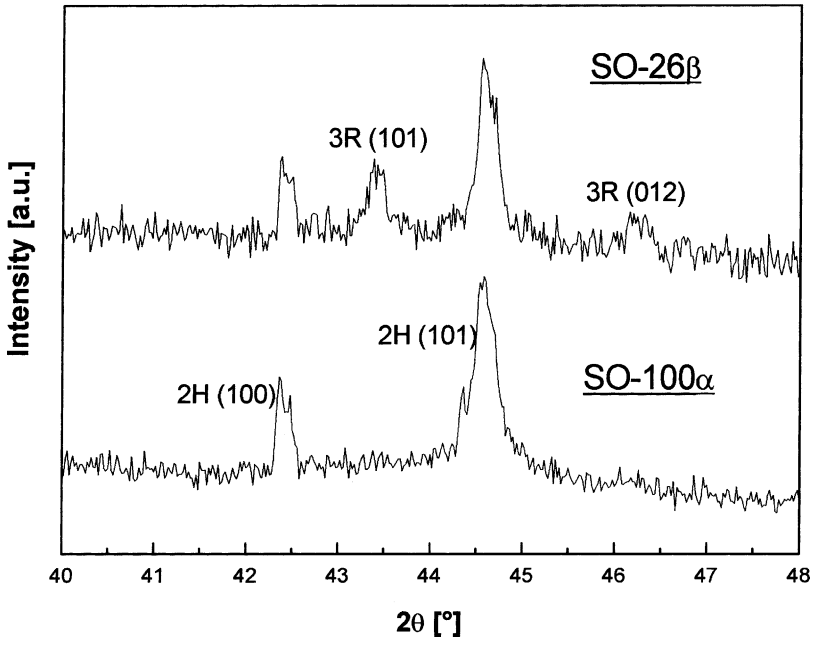

Fig. 2. X-ray diffraction patterns of the graphites SO-26β and SO-100α. The lower XRD pattern shows only the (1 0 0) and (1 0 1) peaks of the hexagonal α-phase, while in the upper XRD diagram the (1 0 1) and (0 1 2) reflections of the rhombohedral β-phase occur additionally. The amount of the rhombohedral and hexagonal modifications was estimated from the integration of the area of their respective (1 0 1) peaks.

SEM investigations have been performed with a LEO DSM 982 Gemini scanning electron microscope (cathode: Schottky emitter). The TEM was done on a TECNAI F 20 especially equipped for high resolution investigations.

3. Results and discussion

3.1. X-ray diffraction

The ratio of the hexagonal and rhombohedral phases can be determined by integration of the peaks (Fig. 2) representing the X-ray diffraction at the (1 0 1) planes of graphite (Fig. 1). We estimated a rhombohedral content of 0% β-phase for the SO-100α and ∼26% β-phase for the SO-26 β. Since the peaks of concern are broad, weak and not very separated from the baseline, this estimation is very rough and there exists some uncertainty about the result for the SO-26β. It is, however, sure that the SO-100α contains no β-phase in the structure, whereas the SO-26β does.

3.2. Anode performance

The relative anode performance has been tested in three different electrolytes: (i) 1 M $LiClO_4$ in EC:DEC (1:1, w:w); (ii) 1 M $LiClO_4$ in EC:DMC (1:1, w:w) and (iii) 1 M $LiClO_4$

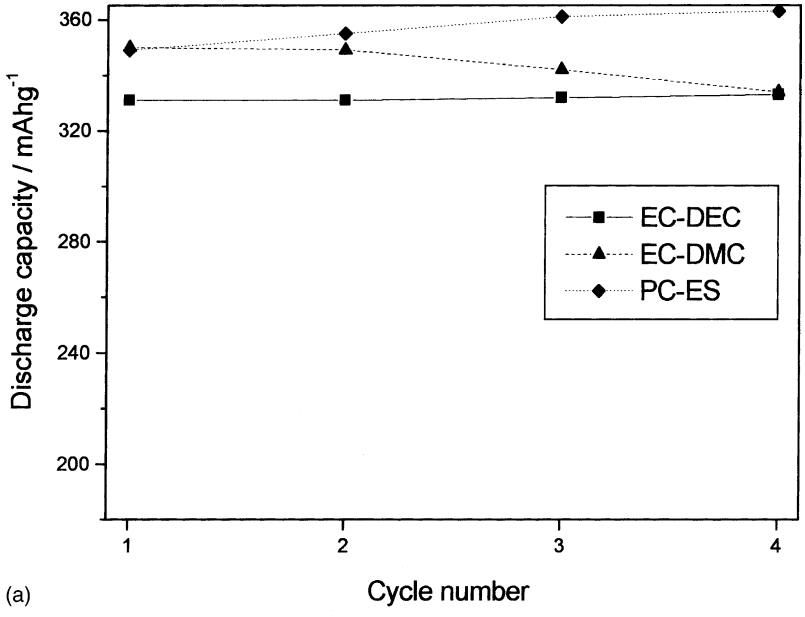

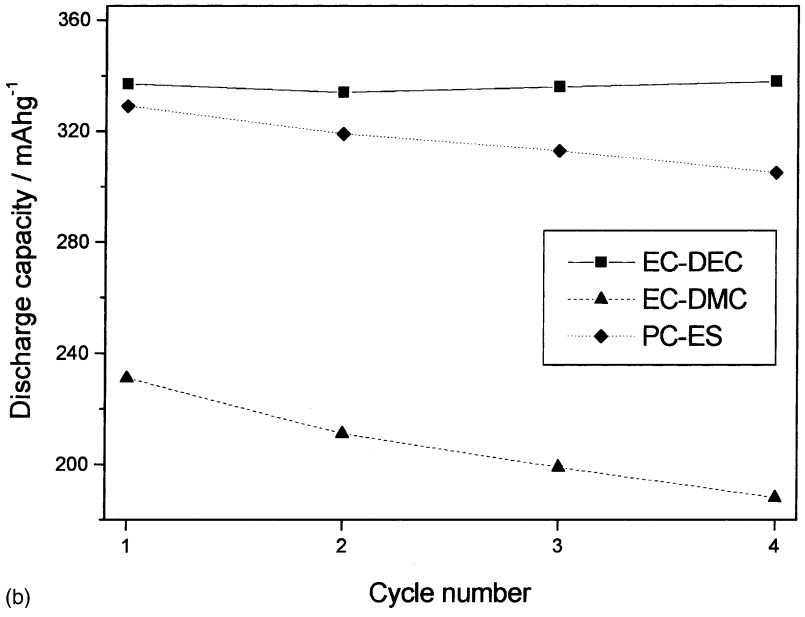

Fig. 3. Discharge capacity vs. cycle number of (a) the graphite SO-26β and (b) the graphite SO-100α in 1 M $LiClO_4$ EC:DEC (1:1, w:w), 1 M $LiClO_4$ EC:DMC (1:1, w:w) and 1 M $LiClO_4$ PC:ES (95:5, v:v) as electrolytes. $i = \pm 20$ mA g^{-1}, cut-off: 24/1500 mV vs. Li/Li^+.

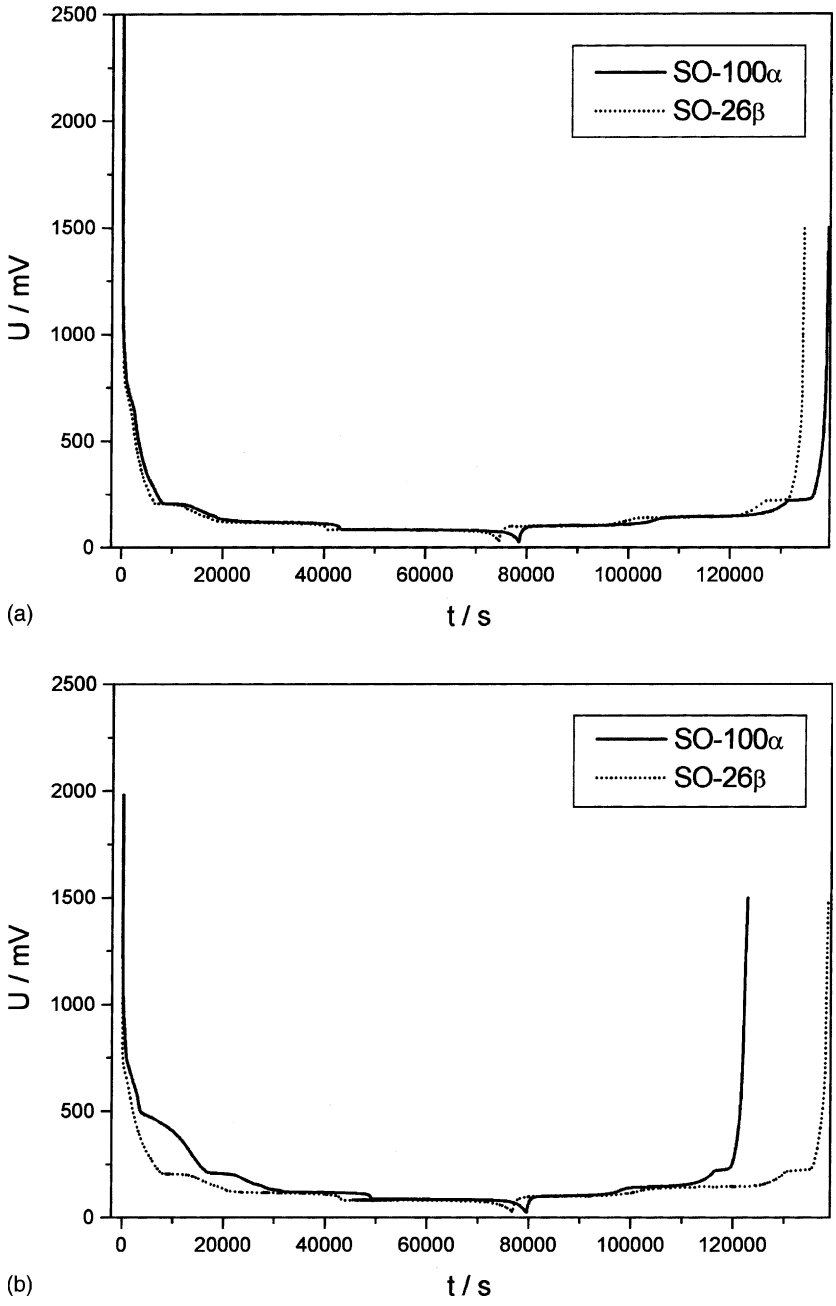

Fig. 4. First cycle charge/discharge curves of the graphites SO-26β and SO-100α in (a) 1 M $LiClO_4$ EC:DEC (1:1, w:w), (b) 1 M $LiClO_4$ EC:DMC (1:1, w:w) and (c) 1 M $LiClO_4$ PC:ES (95:5, v:v). $i = \pm 20$ mA g^{-1}, cut-off: 24/1500 mV vs. Li/Li^+. The discharge/charge efficiencies are: (a) in EC:DEC 80% (SO-26β), 77% (SO-100α); (b) in EC:DMC 80% (SO-26β), 55%. (SO-100α); and (c) in PC:ES 70% (SO-26β), 55% (SO-100α).

in PC:ES (95:5, v:v). In practical cases, EC based electrolytes are reduced within a certain potential range, and within this potential range solvent co-intercalation can take place [11–13] also.[3] Roughly said, the used EC electrolytes may be considered as indicators for those differences in structural disorder, which allow or suppress solvent co-intercalation.

For the PC:ES electrolyte it has been reported [14] that the film forming electrolyte additive ES successfully suppresses solvent co-intercalation into graphite. Electrolyte reduction and SEI formation already starts at ~2 V versus Li/Li^+ and when the graphite electrode reaches the potentials of solvent co-intercalation, it is already protected by an effective SEI film, which does not allow the solvated lithium cations to penetrate into the graphite. The extent of reduction in this electrolyte can be considered to depend on the properties of the graphite surface, such as surface area and surface morphology.

[3] For a detailed discussion of the reaction "solvent co-intercalation" and subsequent reactions, which affect the graphite anode performance, we like to refer the reader to [11–13].

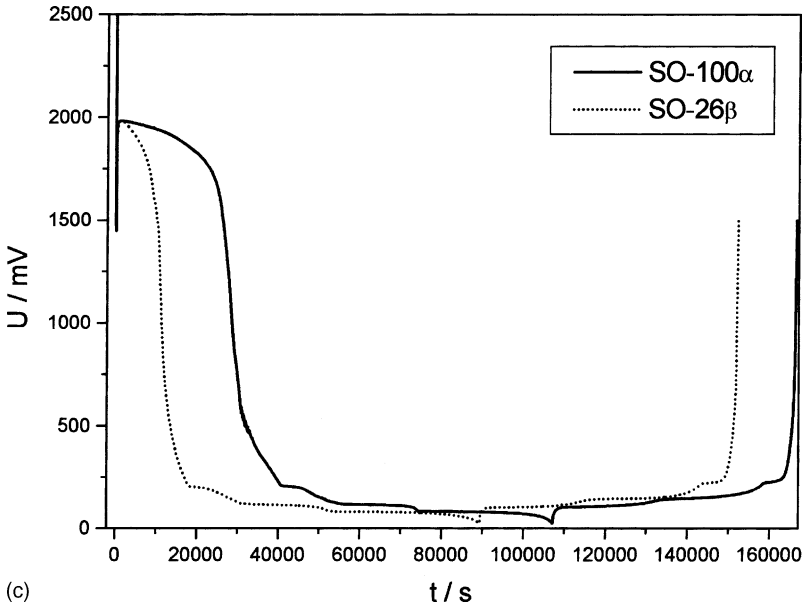

Fig. 4. (*Continued*).

In conclusion, in first approximation, electrolytes, which are either more sensitive to graphite bulk properties (EC-based) or more sensitive to graphite surface properties (PC:ES-based), have been chosen.[4].

The differences in the discharge capacities during cycling (Fig. 3) as well as in the shape of the 1st cycle charge/discharge curves (Fig. 4) are significant, not only when different graphites, but also when different electrolytes are compared. The SO-26β (Fig. 3a) shows high and stable discharge capacities in the EC:DEC and PC:ES electrolytes. In contrast, there is some slight capacity fading in the EC:DMC electrolyte, though the 1st cycle discharge capacity is high, too.

With the SO-100α (Fig. 3b) only in the EC:DEC electrolyte high and constant discharge capacities are achieved. In PC:ES the equally high discharge capacity in the 1st cycle shows a rapid fading in the following cycles. The performance in the EC:DMC electrolyte is the worst, as both poor discharge capacities and strong capacity fading are observed.

It should be emphasised, that for certain electrolytes, independent of the presence of structural disorder, e.g. rhombohedral phase or grain boundaries, high discharge capacities can be achieved with both graphites.

The charge/discharge curves performed in the EC:DEC electrolyte (Fig. 4a) basically look the same. There seems to be no striking influence of the different graphite structures on the electrochemical performance in the EC:DEC electrolyte. On the other hand, both, in the EC:DMC (Fig. 4b) and in the PC:ES electrolyte (Fig. 4c), the SO-100α graphite displays significantly lower 1st cycle discharge/charge efficiencies than the SO-26β. The strong differences in the shape of the charge/discharge curves (Fig. 4b and c) reveal that these poor efficiencies in the EC:DMC and PC:ES electrolyte are due to different effects.

Whereas the EC:DEC electrolyte apparently does not strongly co-intercalate into graphite, the EC:DMC electrolyte does. The charge curve of the SO-100α graphite shows an additional plateau starting at potentials below 550 mV versus Li/Li^+, which indicates extensive co-intercalation. A difference in the filming behaviour of the two graphites, however, is already observed at higher potentials. In comparison to the SO-26β, twice the charge capacity is consumed for the SO-100α in order to reach the potential of 550 mV versus Li/Li^+. The differences of the 1st cycle efficiencies are even more significant (Fig. 4b and c). In agreement with previous reports, we could confirm strong solvent co-intercalation for the graphite with the lower rhombohedral phase content and the corresponding lower number of defects. Solvent co-intercalation and subsequent reduction inside the graphite obviously increases the irreversible capacities because surfaces inside the graphite take part in the SEI formation process, too. The discharge capacities are decreased, which may be due to loss of active graphite material by partial graphite destruction (exfoliation) or by partial blocking of lithium storage sites inside the graphite by SEI films.

With regard to the efficiencies, similar tendencies for EC:DMC could be found for the PC:ES electrolyte. Compared to the SO-26β, with the SO-100α approximately twice the charge is consumed for reaching the lithium intercalation plateau potentials at approximately 250 mV versus Li/Li^+. The reason for this poor efficiency, however, is completely

[4] It can, however, not be excluded that the differences in the graphite surface have also in EC-based electrolytes some influence on the performance. The same is true for possible influences of the graphite bulk in PC:ES based electrolytes.

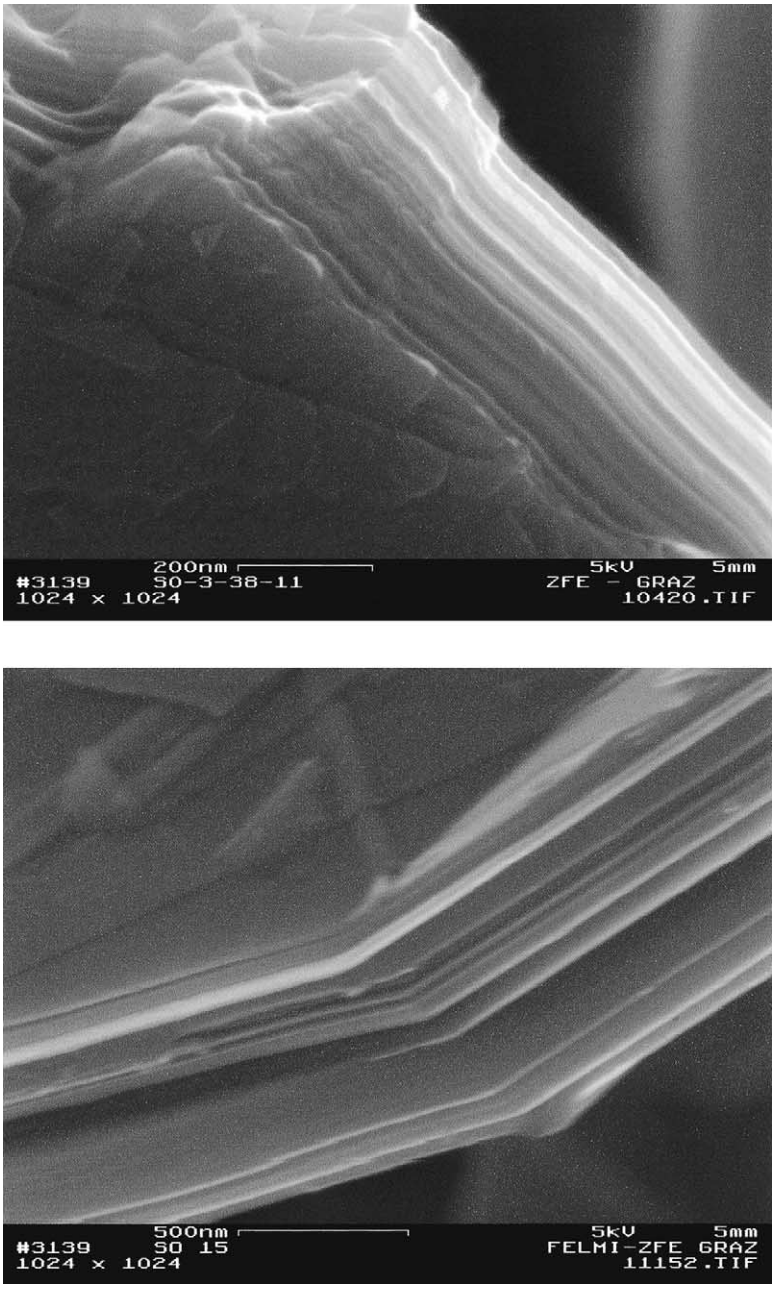

Fig. 5. SEM pictures of (*top*) the graphite SO-26β and (*bottom*) the graphite SO-100α.

different. In PC:ES, SEI filming proceeds predominantly at 2 V versus Li/Li^+, i.e. at potentials far more positive than the potential of solvent co-intercalation. Therefore, one should expect a film formation process, which primarily depends on the graphite surface properties.[5] However, the differences can not be simply related to the BET specific surface areas, as these are very similar: SO-26β (4.6 $m^2\ g^{-1}$) and SO-100α (5.0 $m^2\ g^{-1}$). Therefore, we investigated the graphite surface properties in detail by means of electron microscopy.

[5] Slight potential fluctuations, which might be correlated to minor co-intercalation reactions, can be observed at 600–400 mV versus Li/Li^+.

3.3. Electron microscopy studies

The impact of the different preparation procedures on the structure of the two graphite samples is well illustrated by SEM (Fig. 5). Mechanical treatment (SO-26β) causes considerable damage at the basal plane surfaces and at the prismatic surfaces. The prismatic surfaces appear rough and the mechanical shearing impact resulted in a movement of the graphene layers, which is visible as a "fan-shaped" arrangement of graphene layers. At contrast, thermal treatment (SO-100α) obviously has the opposite influence. The basal plane surface appears quite intact and the prismatic surface morphology is smooth. Furthermore, at the prismatic

surfaces, the graphene layer packages appear considerably thicker.

High-resolution TEM is able to provide atomic resolution and discloses the differences in microstructure of the graphite samples. The bulk structure of the SO-26β (Fig. 6) is quite disordered and shows stacking faults and slight bending of the graphene layers. At the borders of the particles, the graphene layers end in even more disordered, almost amorphous looking structures. (Fig. 6). This ''sub-surface'' layer (part of the graphite bulk at the border of the particle near the surface) is approximately 1 nm thick. Moreover, it is very probable, that the strong disorder of the ''sub-surface'' and not the apparently much lesser disorder of the rest of the bulk graphite particle, is responsible for the suppression of solvent co-intercalation in the EC:DMC based electrolyte.

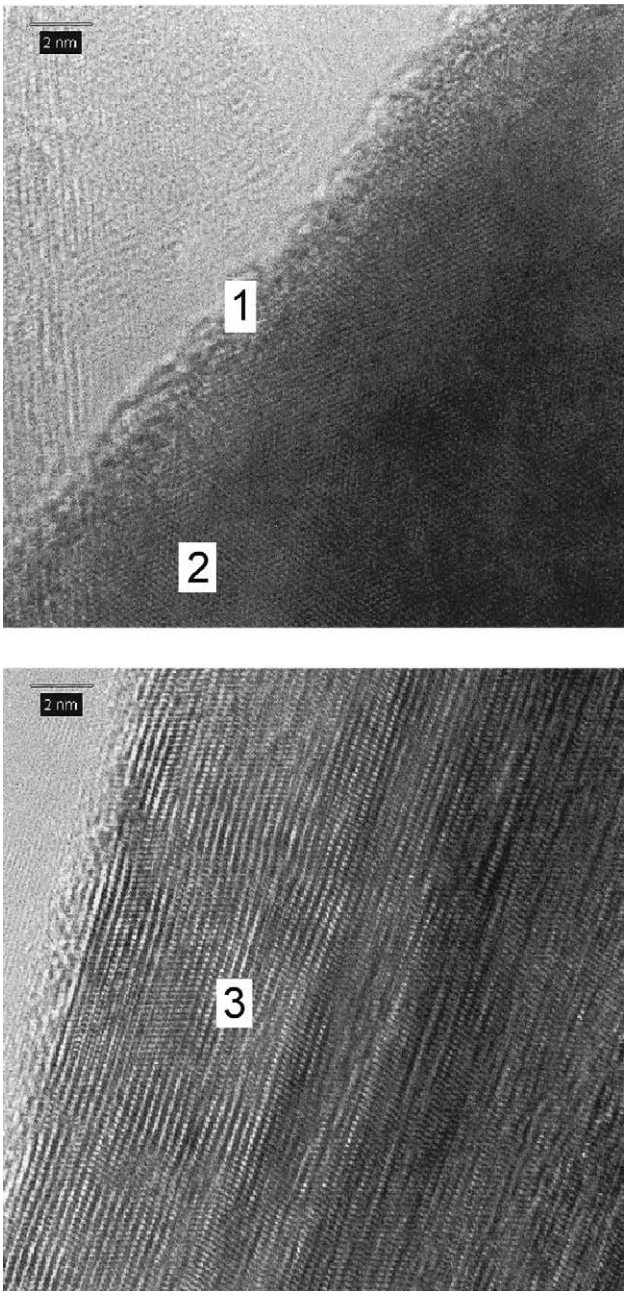

Fig. 6. TEM pictures of the graphite SO-26β. (*Top*): The basal plane surface reveals a highly disordered ''sub-surface'' layer at the border of the particle (1). The observation of the C–C distance of 0.14 is indicating atomic resolution (2). (*Bottom*): The interlayer distance of graphite is visible. There is considerable disorder (bending and dislocations) in the graphite bulk. The highly disordered ''sub-surface'' layer is visible again (3).

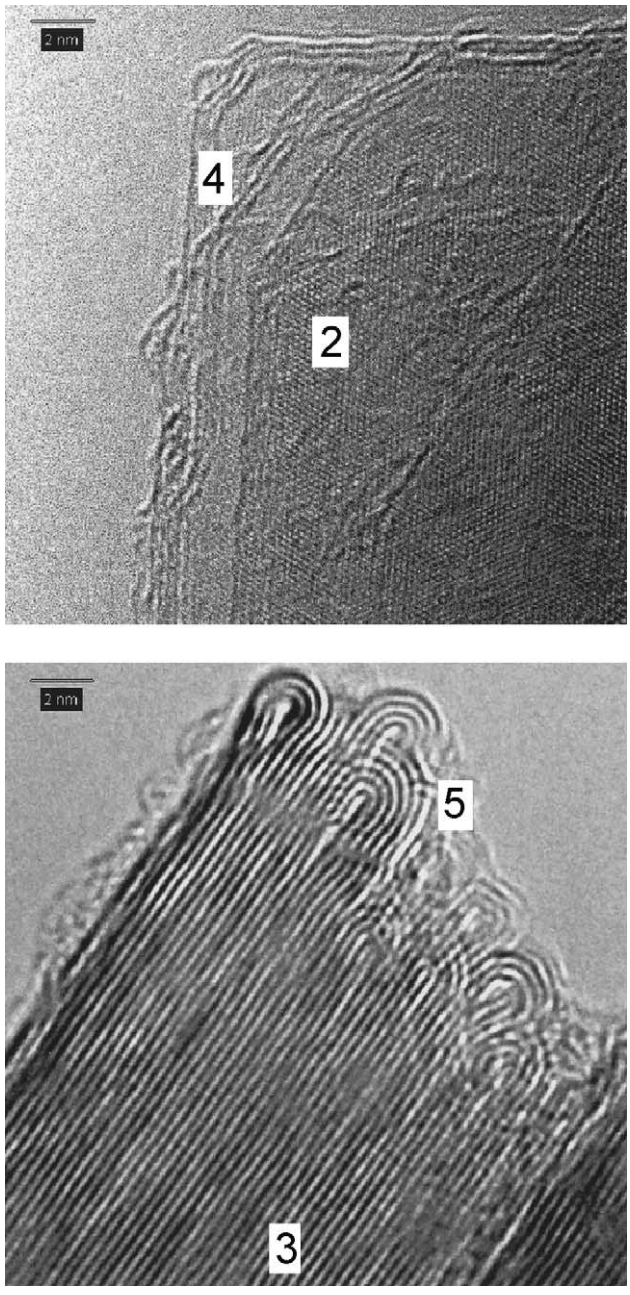

Fig. 7. High resolution TEM pictures of the graphite SO-100α. (*Top*): The C–C distance of 0.14 at the basal plane is clearly visible (2). At the border of the particle very unique structures appear (4). (*Bottom*): The graphene layers are folded near at prismatic surfaces. Closed, partly closed and open structures can be recognised (5). In contrast to the SO-26β, the graphene layers show a high degree of order (3). Again, the interlayer distance of 0.34 can be seen.

Very unusual round-shaped (convoluted or folded) graphene layer structures could be determined by TEM at the prismatic surfaces of the SO-100α graphite (Fig. 7). Closed, partly closed and open formations can be recognised, with microstructures resembling ''fingerprints''. Similar structures are known from ''onion-like''-textured carbon fibres, carbon nanotubes or fullerenes, but to our knowledge have, so far not been observed for highly graphitic carbon materials, such as natural graphites. A view at the bulk reveals a well-developed crystal structure and a high stacking order. The high order, both in the bulk and at the surface apparently creates no strong mechanical hindrance for suppression of solvent co-intercalation, which explains the results obtained in the EC:DMC electrolyte.

It has been proposed previously [14,15], that different graphite surface morphologies (in particular at the prismatic surfaces) have a strong influence on the SEI deposition process. The interaction of SEI products with the graphite surface and the fixation (''anchoring'') of the products to the surface can be expected to be completely different for the two graphites. Obviously, the disordered surface of the SO-26β sample induces a much more effective SEI filming than the well-ordered and partly convoluted prismatic surface of the SO-100α graphite. In addition, one can assume, that for these different surfaces, the electronic conductivity and thus also the electron transfer in the electrolyte strongly varies and hencefore the rate for electrolyte decomposition and SEI formation varies, too. This might explain the large differences in efficiencies observed in the PC:ES electrolyte, with its extent of reduction at 2 V versus Li/Li^+ primarily depending on graphite surface properties.

4. Conclusions

Two very different natural graphite-based carbon samples have been investigated. The graphite, which has been processed by strong mechanical impact contains a larger amount of rhombohedral phase and also has a higher defect concentration in the structure. The natural graphite, which has been processed by thermal annealing at elevated temperatures contains no rhombohedral phase and a low defect concentration. The anode performance of the graphites with (SO-26β) and without (SO-100α) rhombohedral phase depends strongly on the electrolyte, as has been shown for EC:DEC, EC:DMC and PC:ES based electrolytes. As a simple rule, a high number of structural defects is beneficial to the performance. It is particularly favourable when a high defect concentration is present in the ''sub-surface'' part of the graphite particle (see further). When an EC:DEC based electrolyte is used, however, satisfactory discharge capacities and discharge/charge efficiencies are also possible with the all-hexagonal (low defect) SO-100α. With an EC:DMC based electrolyte the effects of the different structures on performance are much more visible. Strong solvent co-intercalation is only observed for the SO-100α, and its anode performance in terms of discharge capacity and efficiency is poor.

In addition to the already known fact that solvent co-intercalation reactions are influenced by the rhombohedral phase content (and corresponding defect concentration), the influence of mechanical or thermal treatments on the graphite surface and the graphite ''sub-surface'' (part of the graphite bulk near the surface) has to be considered for the explanation of the SEI formation processes, as well. This is particularly true for the prismatic surfaces, where solvated and unsolvated lithium intercalation takes place. Whereas the ''sub-surface'' of the partially rhombohedral graphite SO-26β is almost amorphous revealing the considerable damage due to mechanical impact, the all-hexagonal graphite SO-100α exhibits highly crystalline and very unique ''fingerprint''-type prismatic surface sites. These surfaces may induce different electrolyte decomposition and SEI deposition processes. The fixation (''anchoring'') of the SEI to the surfaces should be very much different, too. This is especially true for the PC:ES electrolyte, whose reduction at high graphite electrode potentials of approximately 2 V versus Li/Li^+ can be expected to be very sensitive to graphite surface properties. We will report on the surface heterogeneities of these graphites in more detail in a forthcoming paper.

Finally, the question remains, (i) whether the beneficial effect of the structural defects/rhombohedral phase is a simple surface or ''sub-surface'' effect, i.e. a thin surface shell of amorphous graphite, which surrounds a highly crystalline all-hexagonal graphite core, would result in similarly good anode performance because solvent co-intercalation is still successfully suppressed, or (ii) whether the presence of the structural defects and/or rhombohedral phase in the graphite bulk has an additional specific influence on anode performance.

Acknowledgements

Support by the Austrian Science Funds through the special research program ''Electroactive Materials'' is gratefully acknowledged. We thank Mitsubishi Chemical Corporation (Japan), Merck (Germany) and Honeywell (Germany) for the donation of samples used in this study.

References

[1] O. Volher, G. Nutsch, G. Collin, F. von Sturm, E. Wege, W. Frohs, K.D. Henning, H. von Kienle, M. Voll, P. Kleinschmitt, in: Carbon–Graphite, Ullmann's Encyclopedia of Industrial Chemistry, sixth ed., Electronic Release, 2002.
[2] H. Huang, W. Liu, X. Huang, L. Chen, E.M. Kelder, J. Schoonman, Solid State Ionics 110 (1998) 173.
[3] K. Guerin, A. Fevrier-Bouvier, S. Flandrois, M. Couzi, B. Simon, P. Biensan, J. Electrochem. Soc. 146 (1999) 3660.
[4] S. Flandrois, K. Guerin, Mol. Cryst. Liq. Cryst. 340 (2000) 493.

[5] S. Flandrois, A. Fevrier, P. Biensan, B. Simon, US Patent No. 5 554 462 (1996).
[6] H. Shi, J. Barker, M.Y. Saiidi, R. Koksbang, L. Morris, J. Power Sources 68 (1997) 291.
[7] B. Simon, S. Flandrois, A. Fevrier-Bouvier, P. Biensan, Mol. Cryst. Liq. Cryst. 310 (1998) 333.
[8] B. Simon, S. Flandrois, K. Guerin, A. Fevrier-Bouvier, I. Teulat, P. Biensan, J. Power Sources 81-82 (1999) 312.
[9] F. Cao, I.V. Barsukov, H.J. Bang, P. Zaleski, J. Prakash, J. Electrochem. Soc. 147 (2000) 3579.
[10] H. Shi, J. Barker, M.Y. Saidi, R. Koksbang, J. Electrochem. Soc. 143 (1996) 3466.
[11] G.H. Wrodnigg, J.O. Besenhard, M. Winter, J. Electrochem. Soc. 146 (1999) 470.
[12] J.O. Besenhard, M. Winter, J. Yang, W. Biberacher, J. Power Sources 54 (1995) 228.
[13] M. Winter, G.H. Wrodnigg, J.O. Besenhard, W. Biberacher, P. Novák, J. Electrochem. Soc. 147 (2000) 2427.
[14] H. Buqa, P. Golob, M. Winter, J.O. Besenhard, J. Power Sources 97-98 (2001) 122.
[15] H. Buqa, R.I.R. Blyth, P. Golob, B. Evers, I. Schneider, M.V. Santis Alvarez, F. Hofer, F.P. Netzer, M.G. Ramsey, M. Winter, J.O. Besenhard, Ionics 6 (2001) 172.